Surface morphology of ultrathin hex-Pr_2O_3 films on Si(111)

H. Wilkens[1], J. Rodewald[1], S. Gevers[1], M.H. Zoellner[2], T. Schroeder[2,3] and J. Wollschläger[a)1]

[1] *Fachbereich Physik, Universität Osnabrück, Barbarastr. 7, D-49069 Osnabrück, Germany*

[2] *IHP, Im Technologiepark 25, D-15236 Frankfurt(Oder), Germany*

[3] *BTU Cottbus, Institute of Physics, Konrad-Zuse-Str.1, D-03046 Cottbus, Germany*

(Dated: 20 December 2012)

In this work the morphology of the surface of hexagonal $Pr_2O_3(0001)$ films grown on Si(111) is studied by high resolution low energy electron diffraction combined with spot profile analysis. For this purpose, praseodymia films prepared by molecular beam epitaxy were capped with protecting amorphous germanium films. After removal of the capping layers due to heating in diluted oxygen atmosphere the surface properties of the oxide film were investigated in-situ with Auger electron spectroscopy and spot profile analysis low energy electron diffraction. The removal of the capping layer has no impact on the hexagonal $Pr_2O_3(0001)$ film structure which is shown by x-ray diffraction. Surface sensitive electron diffraction confirms that the surface of the oxide film has hexagonal structure. Diffraction spot profile analysis shows that the film surface has grain structure without any mosaic spread due to the negligible lateral lattice mismatch between hexagonal $Pr_2O_3(0001)$ and Si(111). In addition, single atomic steps with complete bulk unit cell height are present at the surface. The density of the atomic steps is small pointing again to the high quality of the surface of hexagonal Pr_2O_3 films compared to cubic Pr_2O_3 films.

[a)] email: joachim.wollschlaeger@uos.de

I. INTRODUCTION

Buffer layers play an important role to manufacture stackings of different materials necessary, e.g., in the fields of micro- and nanoelectronics. Here, for economic reasons, it is necessary to find insulating epitaxial buffer materials which are lattice matched to Si as substrate material to use the well established technologies developed to make structures based on the Si platform. For instance, the integration of Ge on insulators (GeOI) is promoted to get access to the higher carrier mobilities of Ge[1,2]. Furthermore, the integration of III-V materials is desired for applications in the fields of optoelectronics and photovoltaics[3].

One well suited candidate for this purpose to obtain insulating epitaxial buffer layers of superior quality are hexagonal praseodymia sesquioxide (hex-Pr_2O_3) films with (0001) orientation since the lateral lattice mismatch is only 0.52% with respect to Si(111). In addition, hex-Pr_2O_3 has the lowest oxygen content and, therefore, it cannot deliver oxygen to oxidize other materials deposited on top as previously demonstrated for epitaxial Si(111) films[4].

Another field of great interest in praseodymia epitaxy is the field of catalysis since praseodymium oxide exhibits the highest oxygen mobility within the rare earth oxides[5]. Therefore praseodymia of different stoichiometry is an interesting candidate for redox based catalysis via the Mars-van-Krevelen mechanism[6]. Simplified model systems like single crystalline thin films are necessary to understand details of these complex catalytic reactions (e.g. oxygen transport).

For all these different applications, it is very important to get deeper insight in the structure and morphology of praseodymia film surfaces, especially of the atomic step density. For instance, in the field of catalysis a high step density is favourable since atomic steps proliferate catalytic reactions. On the contrary, they are disadvantageous regarding the use as buffer layer since very smooth surface are needed in epitaxial growth.

Single crystalline growth of hexagonal praseodymium sesquioxide (hex-Pr_2O_3) films with (0001) orientation on Si(111) substrates was first achieved by Tarsa et al. using pulsed laser deposition (PLD)[7]. Later the crystalline quality of hex-Pr_2O_3(0001)/Si(111) structures grown by molecular beam epitaxy (MBE) were extensively studied[8,9]. The structure of monolayers of hex-Pr_2O_3(0001) deposited on Si(111) has been solved by grazing incidence x-ray diffraction (GIXRD) studies[10].

Nevertheless, there is only a very limited number of surface studies on praseodymia films available up to now which focus on praseodymia monolayers on Si(111)[9,11,12]. Therefore, it is necessary to perform surface studies on thicker high quality films beyond praseodymia monolayers.

These films, however, have usually to be transfered to surface characterization chambers through ambient conditions. Here, the formation of hydroxides ($Pr(OH)_3$) under ambient conditions is very disadvantageous[13,14]. Previous investigations of praseodymia films with cubic phase on Si(111) show that $Pr(OH)_3$ is only formed at the topmost layers of the oxide film while the bulk of the praseodymia film is rather stable[15]. The conversion $Pr_2O_3 \rightarrow Pr(OH)_3$, however, is much easier for the hexagonal structure since both species exhibit hexagonal crystal symmetry so that the Pr cations have only to be slighty reordered to form the hydroxide[16,17].

Up to now amorphous Si capping layers were mainly used as protecting capping layers[18]. These layers, however, are difficult to remove and change the surface properties (e. g. argon sputtering roughens the surface). The work presented here investigates amorphous germanium (a-Ge) as an alternative capping layer since Ge films can thermally be removed in very diluted oxygen atmosphere so that the praseodymia is probably not attacked as observed for other techniques, e.g. ion milling.

In the following, first, we study both the thermal removal of Ge capping layers from hex-Pr_2O_3(0001) films in thin oxygen atmosphere as well as the stability of the hex-Pr_2O_3(0001) films. Thereafter, we present a detailed surface analysis of the morphology of the hex-Pr_2O_3(0001) surface.

II. EXPERIMENT

A 9.3 nm single crystalline hex-Pr_2O_3(0001) film was grown on Boron doped Si(111) wafer according to the recipe reported by Ref.[9,19]. Afterwards, an a-Ge capping layer with thickness 8.5 nm was deposited at room temperature to protect the hex-Pr_2O_3 film from degeneration under ambient conditions. Having transfered the wafer to ambient conditions, layer thicknesses were determined using *ex-situ* x-ray reflectivity (XRR) while the crystalline quality of the hex-Pr_2O_3 film was monitored by x-ray diffraction (XRD).

After loading the samples into a ultra high vacuum (base pressure 10^{-10} mbar) the cap-

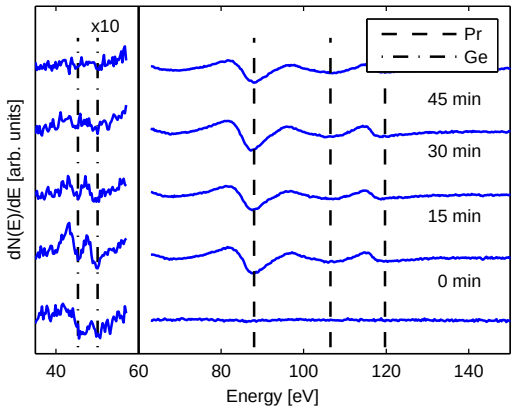

FIG. 1. Derived AES spectra for different exposure times to 10^{-6} mbar oxygen atmosphere at 500°C sample temperature. After 15 min exposure strong praseodymium peaks become visible, while the germanium peak completely vanishes after 60 min O_2 exposure.

ping Ge layers were carefully removed in thin oxygen atmosphere via heating of the entire structures. The varied parameters were oxygen partial pressure ($p(O_2) \leq 10^{-5}$ mbar), sample temperature (300°C - 500°C) and exposure time to oxygen atmosphere (99.998 % O_2). Annealing was performed by resistive heating and temperature was controlled with an IR pyrometer.

The removal process was monitored by Auger electron spectroscopy (AES) and spot profile analysis low energy electron diffraction (SPA-LEED) measurements performed after each annealing step. Having prepared the bare surface of the hex-Pr_2O_3 films the surface morphology was studied by SPA-LEED. Therefore, a spot profile analysis of the specular diffraction spot for different electron energies was performed.

Afterwards the samples were recapped with amorphous Si at room temperature and transfered to beamlines W1 and P08 at DESY (Hamburg, Germany) to inspect the integrity of the structure of the hex-Pr_2O_3 films by (GI)XRD measurements. Both beamlines are equipped with six circle diffractometers to perform these studies. Photon energies of 10 keV and 10.5 keV were used at P08 and W1, respectively.

III. RESULTS

A. Removal of Ge capping layer

Preliminary investigations on the removal of germanium capping layers with different sample temperatures and oxygen pressures starting at 300°C and 10^{-8} mbar with one hour exposure time were performed to find the lower desorption limits (not shown here). The temperature was increased in 50°C steps and the oxygen partial pressure in decade steps. The upper limits for process parameters to remove the Ge capping layer are given by the phase transition of the underlying hex-Pr_2O_3 film to keep the hexagonal structure of the oxide film. Schroeder et al.[18] reported that the transition hex-Pr_2O_3 → cub-Pr_2O_3 occurs at 450°C and 10^{-5} mbar oxygen pressure. Since we are searching a removal method with no impact on the underlying oxide film these are the upper limits for processing the film structures.

The preliminary AES investigations show that the desorption at 350°C starts at a relative high oxygen pressure of 10^{-5} mbar. This temperature is sufficiently lower than the critical temperature for the irreversible phase transition. At least 10^{-7} mbar oxygen is necessary to remove Ge from the surface at 400°C annealing temperature. Complete removal of the germanium film is achieved at 500°C and 10^{-6} mbar oxygen pressure which is below the critical pressure to initiate the transition hex-Pr_2O_3 → cub-Pr_2O_3 as shown below.

Fig. 1 shows the derived AES spectra obtained after exposing the samples to 10^{-6} mbar oxygen atmosphere at 500°C for different times. The characteristic Ge peaks are located at 47 eV and 52 eV electron energy while further Ge peaks are too weak to be detected[20]. The Pr peaks are located at 87 eV, 106 eV and 119 eV.

After the first desorption cycle strong Pr peaks appear while the Ge peaks are still visible. Since the inelastic free path of the Pr Auger electrons is smaller than 1 nm we conclude, that major parts of the Ge film are already removed after the first desorption step.

This result is supported by the SPA-LEED studies. While the a-Ge capped films do not show any diffraction pattern due to the amorphous structure of the capping layer a hexagonal diffraction pattern already appears after the first 15 min removal step of Ge. Since electron diffraction is very surface sensitive, this diffraction pattern shows that large parts of the bare hex-Pr_2O_3 surface must have been formed although there is still Ge detected in the

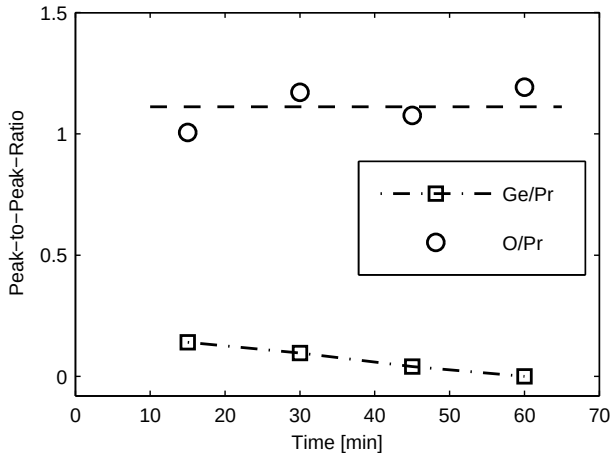

FIG. 2. Oxygen (503 eV)/ praseodymium (87 eV) and germanium (503 eV) / praseodymium (87 eV) peak-to-peak ratio against exposure time. The Pr/Ge ratio decreases continuously while the O/Pr ratio is constant.

AES spectra (cf. Fig. 1). Therefore, the residual Ge must have formed small islands.

Since residual Ge can still be detected it takes further annealing cycles to remove it from the surface (cf. Fig. 2). The Ge (503 eV)/Pr (87 eV) peak-to-peak ratio has been determined to quantify the Ge desorption process. It decreases continuously in time and Ge is removed after 60 min of exposure

A strong oxygen Auger electron peak is still visible after 15 min. This oxygen content, however, is attributed to the praseodymium oxide instead of the Ge oxide since Fig. 2 demonstrates that the O (503 eV)/Pr (87 eV) ratio is almost constant during the entire removal process. The latter fact indicates that no change of the stoichiometry for the surface near region of the praseodymia film takes place.

B. Stability of hex-Pr_2O_3 film during thermal processing

Further (GI)XRD experiments were performed to verify that the film structure is not changed neither due to the reactive removal of the Ge capping layer nor due to the exposure of the hex-Pr_2O_3 to 10^{-6} mbar O_2 at 500°C for one hour. Therefore, synchrotron based experiments were performed on both the non-modified a-Ge/hex-Pr_2O_3/Si(111) structure and, for comparison, on the same layer structure after Ge removal and recapping with a-Si.

Fig. 3 shows the crystal truncation rod (CTR) scans of the (00)-rod and the (10)-rod measured by XRD for the untreated sample and the sample recapped after Ge removal. The

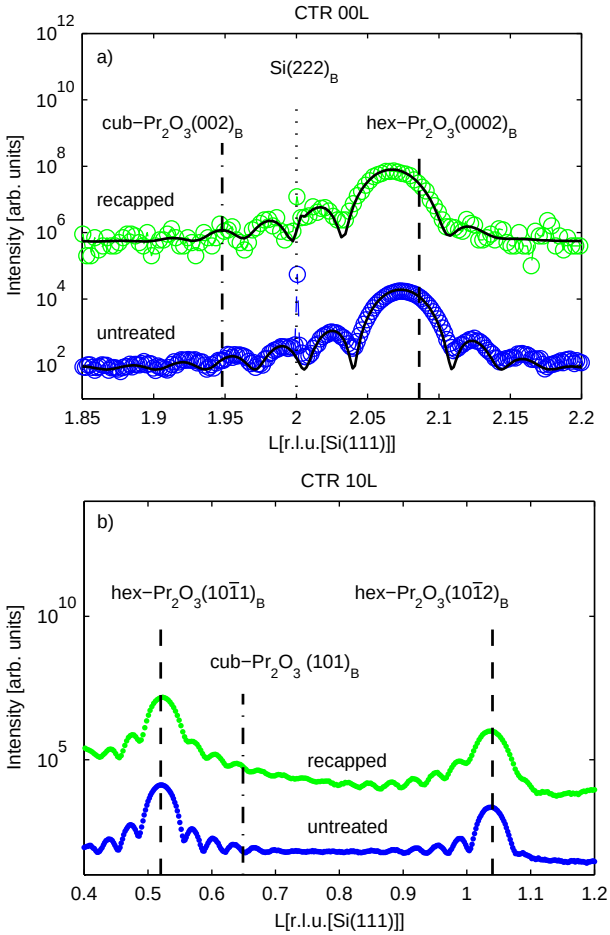

FIG. 3. CTR-scans of the $(00L)_S$-rod a) and $(10L)_S$-rod b) for the untreated sample (blue) and the recapped sample after germanium desorption (green). The structure of the hex-Pr_2O_3 film has not changed. Simulations of the $(0002)_B$ peak within the kinematic diffraction theory (solid lines in a)) show a slightly increase of the surface roughness. Also it has to be emphasized that there is no sign of B-oriented cub-Pr_2O_3.

scattering vector is normalized to the reciprocal lattice units [r.l.u.] of the silicon substrate. Thus the normal component $K_\perp$ is defined via $K_\perp = 2\pi L/c_{\mathrm{Si}}$ where $c_{\mathrm{Si}} = 3.1354$ Å denotes the Si(111) layer spacing. For the $(00L)$ CTR, here the region near the $\mathrm{Si}(222)_B$ Bragg peak is presented, where the subscript B denotes bulk coordinates.

The non-spherical electron density distribution of the Si atoms leads to little intensity of the $\mathrm{Si}(222)_B$ Bragg peak which is forbidden in kinematic diffraction theory. This peak is very sharp due to the large number of crystalline layers involved. Since its small intensity, however, leads to negligible interference effects between substrate and film, the Si peak can be used to calibrate the diffraction measurement (cf. dotted line in Fig. 3).

Well resolved broad Bragg peaks due to the praseodymia films are observed for both

samples. These Bragg peaks are broadened due to the finite thickness of the praseodymia films. The positions of the Bragg peaks is much closer to the expected position of the Bragg peak of hex-Pr_2O_3(0001) (dashed line) than cub-Pr_2O_3(111) (dashed-dotted line). Assuming kinematic diffraction theory we calculated the diffracted intensity of the praseodymia films (solid lines) assuming a hex-Pr_2O_3(0001) unit cell and varying the vertical lattice constant ($c_{\mathrm{bulk}} = 6.01$ Å). The vertical lattice constant $c_{\mathrm{untreated}} = (6.05 \pm 0.02)$ Å and $c_{\mathrm{treated}} = (6.07 \pm 0.02)$ Å are determined for the untreated and recapped sample, respectively. Thus, both values demonstrate that there is no structural change of the hex-Pr_2O_3(0001) film during the desorption process. Also further characteristic hex-Pr_2O_3(0001) peaks at L=0.52, 1.04 and 1.56 are visible in the (00L) CTR (not shown).

In addition, clear fringes are observed in Fig. 3. They are caused by the very homogeneous finite film thickness of both praseodymia films so that the thickness of the crystalline parts of the films can be determined. Our kinematic diffraction analysis (solid lines) excellently describes details of the experimental data, e.g. fringes. For both samples the film thickness is determined to 9.1 nm. This value agrees well with the thickness of 9.3 nm gained from the XRR measurements for the untreated praseodymia film (not shown). Thus, no parts of the praseodymia film are consumed during the formation and desorption of GeO. The slightly higher damping of the fringes for the recapped sample indicates a slightly higher roughness of the praseodymia film after desorption of the Ge capping layer compared to the untreated sample. The untreated sample exhibits an interface and surface roughness of the praseodymia film of $\sigma_{\mathrm{untreated}}$=4.6 Å and the recapped sample $\sigma_{\mathrm{treated}}$=5.3 Å, respectively.

The (10L) CTRs show that exclusively hex-Pr_2O_3 diffraction peaks can be observed for both praseodymia films since hex-Pr_2O_3 fulfills the Bragg conditions at $L \approx 0.52$ and 1.04. Schroeder *et al.* have shown that cub-Pr_2O_3 exclusively shows B-type stacking on Si(111)[18]. Therefore, a Bragg peak of cub-Pr_2O_3 (B-oriented) is expected at $L \approx 2/3$. At this position in reciprocal space, however, no Bragg peak is observed. Thus, for the entire film, a phase transition hex-Pr_2O_3 $\rightarrow$ cub-Pr_2O_3 can also be excluded from these measurements.

C. Surface morphology of the hex-Pr_2O_3 film

Having removed Ge from the praseodymia film, the morphology of the oxide film is characterized by SPA-LEED. Fig. 4 shows the hexagonal electron diffraction pattern of

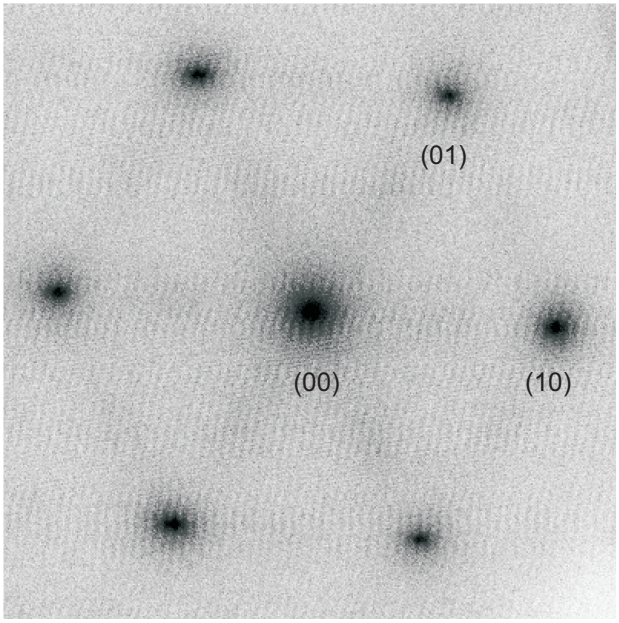

FIG. 4. SPALEED pattern obtained at electron energy 66.5 eV close to in phase after the germanium capping was removed. Very weak streaks between the main diffraction spots are visible.

the praseodymia film obtained close to in phase at an electron energy of 66.5 eV. Changing the electron energy, the diffraction pattern always shows hexagonal symmetry for the arrangement of the diffraction peaks which can be attributed to the (1×1) structure of hex-Pr_2O_3(0001). Because of the surface sensitivity of LEED this indicates that the surface near region has also kept its original structure of the hex-Pr_2O_3(0001)/Si(111) film also after deposition and removal of Ge since more diffraction peaks are expected for cub-Pr_2O_3(111) (bixbyite structure) which has an almost fourtimes larger size of the surface unit cell compared to hex-Pr_2O_3(0001).

In addition, very weak diffraction streaks can also be observed between the main diffraction spots indicating that very small parts of the surface exhibit a badly ordered superstructure. Possible explanation for this superstructure are very small amounts of residual germanium below AES resolution or negligible parts of cub-Pr_2O_3 at the film surface. Since these streaks are very weak, we conclude that the overwhelming part of the surface is hex-Pr_2O_3(0001).

After Ge removal a spot profile analysis of the (00) diffraction spot was performed using cross sections (line scans) in the direction of the (01) diffraction spot (cf. Fig. 5). The diffraction pattern is normalized to the (surface) Brillouin-zone size (BZ) of the hexagonal Pr_2O_3 surface (lateral row distance $a = 3.342$Å). Two Lorentzian functions are necessary to

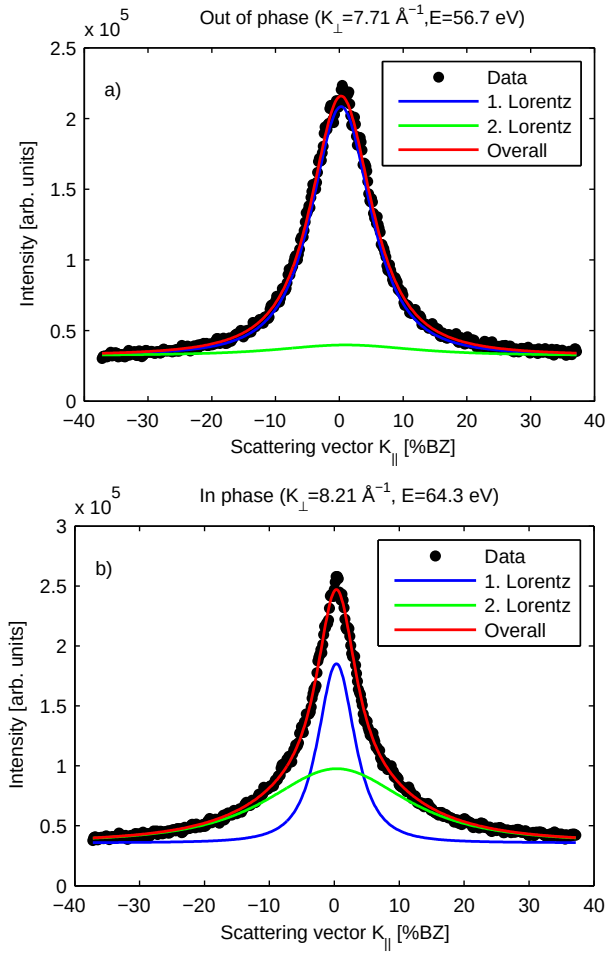

FIG. 5. Line scans through the (00) diffraction spot of the praseodymia film for a) out-phase and b) in-phase scattering conditions. Solid lines correspond to the Lorentzian fit functions.

fit the data. The FWHM of the first smaller Lorentzian varies periodically with scattering vector $K_\perp$ while the second broad Lorentzian shoulder has a constant FWHM of 25 % BZ. These findings show that the first sharp peak is influenced by atomic steps with exponentially decaying terrace size distribution while the shoulder is caused by inhomogeneities (e.g. point defects) or lattice distortions[21].

The FWHM analysis of the sharp peak is shown in Fig. 6. An oscillating behavior of the FWHM is visible which is explained by single layer step heights, since it follows:

$$\mathrm{FWHM}(K_\perp) = 100\%\mathrm{BZ}\frac{a\sqrt{2^{2/3}-1}}{\pi}\left(\frac{1-\cos(dK_\perp)}{\langle\Gamma\rangle}+\frac{1}{D_{\mathrm{lat}}}\right). \quad (1)$$

Here, the step height and the mean terrace width are denoted by d and $\langle\Gamma\rangle$, respectively. The additional offset is needed due to the formation of grain boundaries in the praseodymia

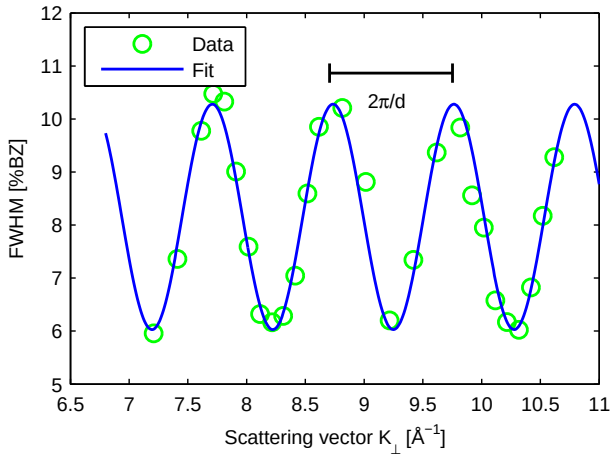

FIG. 6. FWHM of central peak against $K_\perp$. The step height d, the mean terrace width $\langle\Gamma\rangle$ and the grain size D_{lat} were determined from the fit (solid line) according to eq. 1.

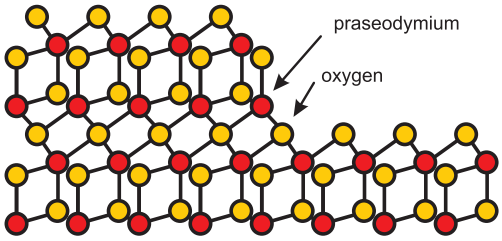

FIG. 7. Vertical step of the hex-Pr_2O_3(0001) surface with step height of one unit cell.

film (average lateral crystallite size D_{lat}). We like to emphasize that we assume a constant offset in eq.(1) since the FWHM at in-phase conditions does not depend on $K_\perp$. This assumption is only justified if the crystallites are not tilted with respect to the normal of the substrate (negligible mosaic spread) as confirmed by our experimental data (cf. Fig. 6). Compared to 1D theory presented in Ref.[22] the prefactor $\sqrt{(2^{2/3}-1)}$ is based on the isotropic exponentially decaying 2D correlation.

Fitting eq.(1) to the experimental data, we determine the step height $d = 6.12$ Å from the periodicity of the FWHM oscillatons. Comparing this value with the values of the vertical lattice distance c of the different Pr_2O_3 phases ($c_{\text{hex-}Pr_2O_3} = 6.01$ Å, $c_{\text{cub-}Pr_2O_3} = 3.22$ Å) as well as with the vertical layer distances determined by XRD in this study we conclude that the step height is in accordance with the complete size of the hexagonal bulk unit cell of hex-Pr_2O_3 (c axis, cf. Fig. 7). Thus, this result demonstrates again that the surface structure of the hex-Pr_2O_3 film was stable under the a-Ge capping layer and against thermal removal of the Ge capping layer.

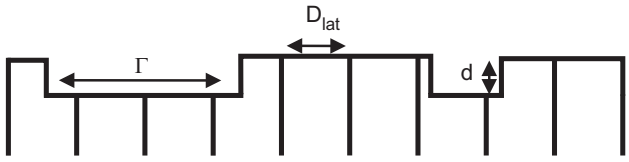

FIG. 8. Surface model derived from the spot profile analysis of the (00) spot for the morphology of the praseodymia film: Smaller grain size D than single step distance $\langle\Gamma\rangle$ so that many of the crystallites are atomically smooth.

Furthermore, the mean terrace width $\langle\Gamma\rangle$ and the average lateral crystallite size D_{lat} are determined from the fitting procedure. We obtain a large mean terrace width of $\langle\Gamma\rangle = 3.7$ nm while the lateral crystallite size of $D_{\mathrm{lat}} = 1.4$ nm in average is smaller. Comparing both values, there are many crystallite surfaces at the surfaces without any steps (cf. Fig. 8).

IV. DISCUSSION

The desorption process of germanium oxide from Ge(001) has been studied extensively in the past. For instance, Hansen and Hudson showed that only GeO species desorb from oxidized Ge samples[23]. Furthermore, they demonstrated that the GeO desorption process follows zero-order kinetics at high oxygen coverages while it becomes first-order at low oxygen coverages due to higher binding energies of GeO at ledge sites. Taking into account the desorption rates reported by them, we conclude in accordance with our results that the overwhelming part of the Ge capping layer is already consumed via GeO formation and desorption during the first annealing step (15min) at 500°C in 10^{-6} mbar O_2. Only small parts of the Ge layer remain on the surface of the praseodymia film as determined by AES. These species are stronger bound to the surface of the praseodymia film probably due to binding at surface defect sites which are, e.g., detected by SPA-LEED (cf. broad shoulder).

In Ref.[24] it was shown that after 2 min heating of a 14 nm GeO_2/Ge at 550°C 10 nm deep voids are formed which expand laterally. We assume that this process also occurs in our case of the Ge capping layer. Voids are generated and the residual Ge forms islands while large parts of the bare surface of the praseodymia film are uncovered. Thus, the measured praseodymia LEED pattern after 15 min exposure can easily be explained. We like to emphasize that the electron diffraction experiment is only sensitive to the Ge-free crystalline praseodymia surface while AES also detects the amorphous germanium.

The very weak streaks in the LEED pattern may indicate some kind of badly ordered

superstructure of the residual germanium with very small domain size or a partial formation of cub-Pr_2O_3. Our XRD results as well as our GIXRD results, however, proof that the praseodymia film has not formed any significant cub-Pr_2O_3 at all. Thus a phase transition can be excluded. In addition, we determined the vertical lattice constant c which agrees well with the vertical lattice constant of hex-Pr_2O_3(0001).

Furthermore, our SPA-LEED investigations show that the atomic steps at the surface have the height d of the vertical bulk lattice constant c. On the one hand, this result agrees well with studies on the growth of hex-Pr_2O_3(0001) on Si(111) by Reflection High Energy Electron Diffraction (RHEED) by Schaefer *et al.*[9]. They demonstrated layer-by-layer growth of the praseodymia film up to 12 nm film thickness where every layer has the height d of the vertical lattice constant c of hex-Pr_2O_3(0001). For the initial growth of hex-Pr_2O_3(0001) on Si(111), the formation of praseodymia islands with full bulk unit cell height has also been observed by Scanning Tunneling Microscopy[11] as well as GIXRD[10]. On the other hand, our investigation differ from SPA-LEED studies on the initial growth of praseodymia on Si(111) at low deposition rates where the atomic step height is approximately half the value determined here[12]. These and other authors, however, report also the formation of additional silicate and silicide at low deposition rates which obviously influences the surface morphology[10,12].

In addition, SPA-LEED studies on cub-Pr_2O_3(111) films on Si(111) showed that the atomic step height of these cubic films is approximately half the step height determined here and, thus, agrees well with vertical lattice plane distance of cub-Pr_2O_3(111)[25,26]. Since these studies also showed the diffraction pattern of cub-Pr_2O_3(111) with its approximately four times larger surface unit cell (bixbyite) we conclude that our preparation of the hex-Pr_2O_3(0001) was successful.

Our SPA-LEED analysis also clearly shows that the hex-Pr_2O_3(0001) film does not show any mosaic spread nor faceting. This finding differs from the results obtained from studies on cub-Pr_2O_3(111) of similar film thickness where the formation of mosaics has been reported[25,26]. These films were formed by the oxygen driven hex-to-cub phase transition or by reduction of PrO_2 films. Gevers *et al.* attribute this effect to the additional lateral stress forced on the praseodymia film during this phase transition due to large differences of their lateral lattice constants. The lateral lattice mismatch of hex-Pr_2O_3(0001) films and cub-Pr_2O_3(111) films with respect to the Si(111) substrate are 0.52% and 2.68%, respectively.

Thus, we demonstrate here that hex-Pr_2O_3(0001) films grow very well on Si(111) due to the negligible lateral lattice misfit. The mean terrace width $\langle\Gamma\rangle$ of 3.7 nm determined here for the hex-Pr_2O_3(0001) is also larger than the corresponding results for cub-Pr_2O_3(111) films where the values are in the range of 0.5-1.5 nm[25,26]. Again, this smoother morphology of the hex-Pr_2O_3(0001) films can be attributed to the much smaller lattice mismatch.

The surface and film morphology of hex-Pr_2O_3(0001) films on Si(111) deduced from our investigation can be summarized by the model presented in Fig. 8. The praseodymia film consists of crystallites which are not tilted with respect to the substrate normal. The surface of the film exhibits only atomic steps with step height d of the vertical lattice constant c of hex-Pr_2O_3(0001). The average step distance (mean terrace width) is larger than the average size of the surface crystallites. Thus, many of the surface crystallites are atomically flat without any atomic step.

V. CONCLUSION

In this work, the surface of hex-Pr_2O_3(0001) films supported on Si(111) was investigated. It was shown that the removal of an amorphous germanium capping layer due to annealing in diluted oxygen atmosphere has no impact on the film structure. So, Ge capping layers are well suited to make surfaces of hex-Pr_2O_3(0001) films accessible to surface science methods as necessary in the fields of model catalysis and epitaxy. We performed a detailed analysis of the hex-Pr_2O_3 film morphology leading to a model with small grain sizes without mosaic spread or faceting. The single atomic steps have the height of the complete bulk unit cell. The average terrace width is larger than the mean surface grain size so that we conclude that many grains do not exhibit any atomic step at all.

VI. ACKNOWLEDGMENT

The authors acknowledge the Deutsche Forschungsgemeinschaft (DFG) via grant no. WO533/16 and SCHR1123/4-1 for financial support. Furthermore, W. Caliebe and C. Deiter are acknowledged during beamline support for synchrotron experiments carried out at HASYLAB/DESY.

REFERENCES

[1]N.A. Bojarzuk, M. Copel, S. Guha, V. Narayanan, E.J. Preisler, F.M. Ross, H. Shang, Appl. Phys. Lett. **83**, 5443 (2003).

[2]J.W. Seo, C. Dieker, A. Tapponnier, C. Marchiori, M. Sousa, J.-P. Locquet, J. Fompeyrine, A. Ispas, C. Rossel, Y. Panayiotatos, A. Sotiropoulos, A. Dimoulas, Microelectron. Eng. **84**, 2328 (2007).

[3]H. Tanoto, S.F. Yoon, W.K. Loke, E.A. Fitzgerald, C. Dohrman, B. Narayanan, M.T. Doan, C.H. Tung, J. Vac. Sci. Technol. B**24**, 152 (2006).

[4]T. Schroeder, P. Zaumseil, G. Weidner, G. Lupina, Ch. Wenger, H.-J. Müssig, J. Appl. Phys. **98**, 123513 (2005).

[5]G. V. Antoshin, K. M. Minachev, D. R. Dmitriev, Russ. Chem. Bull. **16**, 1793 (1967).

[6]Y. Borchert, P. Sonström, M. Wilhelm, H. Borchert, M. Bäumer, J. Phys. Chem. C **112**, 3054 (2008).

[7]E. J. Tarsa, J. S. Speck, McD. Robinson, Appl. Phys. Lett. **63**, 539 (1993).

[8]J. P. Liu, P. Zaumseil, E. Bugiel, H. J. Osten, Appl. Phys. Lett. **79**, 671 (2001).

[9]A. Schaefer, T. Schroeder, G. Lupina, Y. Borchert, J. Dabrowski, Ch. Wenger, M. Bäumer, Surf. Sci. **601**, 1473 (2007)

[10]N.M. Jeutter, W. Moritz, A. Sidorenko, A. Stierle, Appl. Phys. Lett. **90**, 062906 (2007).

[11]L. Libralesso, T. Schroeder, T.-L. Lee, J. Zegenhagen, Surf. Sci. **598**, L347 (2005).

[12]A. Schaefer, V. Zielasek, Th. Schmidt, A. Sandell, M. Schowalter, O. Seifarth, L.E. Walle, Ch. Schulz, J. Wollschläger, T. Schroeder, A. Rosenauer, J. Falta, M. Bäumer, Phys. Rev. B **80**, 045414 (2009)

[13]J. M. Haschke, L. Eyring, Inorg. Chem.**10**, 2267 (1971).

[14]Z.C. Kang, L. Eyring, J. Solid State Chem. **75**, 60 (1988).

[15]S Gevers, T Weisemoeller, D Bruns, A Giussani, T Schroeder, J Wollschläger, J. Phys.: Condens. Matter **23**, 115904 (2011)

[16]I. Khidirov and V. T. Om phys. stat. sol. A **140**, 59 (1993).

[17]O. Greis, R. Ziel, B. Breidenstein, A. Haase and T. Petzel J. Alloys Compd. **216**, 255 (1994).

[18]T. Schroeder, P. Zaumseil, G. Weidner, Ch. Wenger, J. Dabrowski, H.-J. Müssig, J. Appl. Phys. **99**, 014101 (2006).

[19]T. Schroeder, T.-L. Lee, L. Libralesso, I. Joumard, J. Zegenhagen, P. Zaumseil, C. Wenger, G. Lupina, G. Lippert, J. Dabrowski, H.-J. Müssig, J. Appl. Phys. **97**, 074906 (2005).

[20]P. W. Palmberg, G. E. Riach, R. E. Weber, N. C. MacDonald, *Handbook of Auger Electron Spectroscopy* (Physical Electronics, Edina, MN, 1972).

[21]J. Wollschläger, J. Falta, M. Henzler, Appl. Phys. A **50**, 57 (1990).

[22]J. Wollschläger, Surf. Sci. **328**, 3 (1995).

[23]D. A. Hansen, J. B. Hudson, Surf. Sci. **292**, 17 (1993).

[24]S. K. Wang, K. Kita, C. H. Lee, T. Tabata, T. Nishimura, K. Nagashio, A. Toriumi, J. Appl. Phys. **108**, 054104 (2010).

[25]S. Gevers, T. Weisemoeller, B. Zimmermann, F. Bertram, C. Deiter, J. Wollschläger, J. Phys. Condens. Matter **21**, 175408 (2009).

[26]S. Gevers, T. Weisemoeller, B. Zimmermann, C. Deiter, J. Wollschläger, phys. stat. sol. C **7**, 292 (2010).